Dependence of Spin Lifetime on Spin Injection Orientation in Strained Silicon Films

J. Ghosh, D. Osintsev, V. Sverdlov, and S. Selberherr
Institute for Microelectronics, TU Wien, Gußhausstraße 27–29/E360, A–1040 Wien, Austria
Email: {ghosh | osintsev | sverdlov | selberherr}@iue.tuwien.ac.at

***Abstract*—The electron spin properties of semiconductors are of huge interest because of their potential for future spin-driven microelectronic devices. Modern charge-based electronics is dominated by silicon, and understanding the details of spin propagation in silicon structures is key for novel spin-based device applications. The peculiarities of the subband structure and details of the spin propagation in surface layers and thin silicon films in the presence of the spin-orbit interaction is under research. We investigate the influence of the spin injection direction on the spin relaxation. Beginning with the four-component wave functions, we show that the surface roughness induced spin intersubband relaxation matrix elements get reduced for an in-plane spin injection compared to perpendicular-plane spin injection, henceforth the corresponding spin relaxation rate (time) is diminished (enhanced). In order to explain this observation we point out that at the spin relaxation hot spots the perpendicular-plane spin injection results in a maximal spin randomization at any in-plane momentum, which increases the spin relaxation rate and decreases the spin lifetime as compared to an in-plane spin injection.**

Keywords*—Spin relaxation in silicon, k·p method, spin injection direction, spin relaxation hot spots, surface roughness.

I. Introduction

THE breath taking increase in performance of integrated circuits has become possible by continuous miniaturization of CMOS devices, but ever increasing technological challenges and soaring costs are gradually guiding MOSFET scaling to an end [1]. This is driving the search for alternative technologies. Using electron spin may help to reduce power consumption and increase the computational speed of modern electronic circuits [2]. Because of the paramount importance of SOI and FinFET 3D technology for technology nodes from the $22\,\mathrm{nm}$ to the $14\,\mathrm{nm}$ nodes and beyond, spin lifetime in such structures is a very relevant issue under inspection. Although alternative channel materials with a mobility higher than in silicon have been mentioned [3], Si appears to be the perfect material for high performance spin-driven applications [4] for several reasons: (**i**) it is composed of nuclei with predominantly zero spin, (**ii**) it is characterized by weak spin-orbit coupling, (**iii**) silicon technology is well established. Moreover combined with the potentially easy integration with CMOS, spintronic devices are expected to be faster and more compact.

The lower estimate for the spin lifetime at room temperature obtained within the three-terminal injection scheme is of the order $0.1 - 1\mathrm{ns}$ [4]. A long spin transfer distance of conduction electrons has been shown experimentally [5], hence spin propagation at such distances combined with a possibility of injecting spin at room [6] or even at elevated temperature [7] makes the fabrication of spin-based switching devices quite plausible in the near future. However, a large experimentally observed spin relaxation in electrically-gated silicon structures could become an obstacle in realizing spin-driven devices [8], therefore, a deeper understanding of the fundamental spin relaxation mechanism in silicon MOSFETs is urgently required.

Shear strain has been traditionally used to boost electron mobility, and a several orders of magnitude enhancement of spin lifetime in (001) oriented films subjected to [110] uniaxial tensile stress has also been demonstrated [9], [10]. In this paper we report the possibility of a further enhancement of the spin lifetime based on the spin injection direction.

We have considered the parameters as described in the table for our computational investigations. The electron concentration is chosen to be $N_S = 10^{12}\,\mathrm{cm}^{-2}$ and the working temperature $T = 300\,\mathrm{K}$. The sample thickness is kept at $t = 1.36\,\mathrm{nm}$. For such an ultra-thin body the surface roughness (SR) based spin scattering dominates over the other mechanisms [9], because the UTB sandwiched structures, where a thin silicon film is placed between two silicon oxides, are more sensitive to surface roughness scattering. The interface between Si and the oxide plays an important role in determining transport, and henceforth SR scattering is an important relaxation mechanism that has to be accounted for in spin relaxation simulations.

II. Model

We investigate the influence of the intrinsic spin-orbit interaction on the spin relaxation matrix elements in (001) silicon structures by using the effective **k·p** Hamiltonian, with the spin degree of freedom, written at the vicinity of the X-point for the two relevant valleys [11], [12] along the OZ-axis in the Brillouin zone. This method accurately describes the electron wave functions in the presence of strain and the spin-orbit interaction. The spin-orbit term [13] couples the states with the opposite spin projections from the opposite valleys. This can produce a large mixing of the up(down)-spin states between the two unprimed degenerate subbands, resulting in spin hot spots [10], [14] characterized by strong spin relaxation. The spin relaxation hot spot [10] conditions are given by:

$$D\varepsilon_{xy} - \frac{p_x\,p_y}{M} = 0 \tag{1}$$

where D is the shear deformation potential, $M^{-1} = m_t^{-1} - m_e^{-1}$ (ref: table), ε_{xy}: the applied shear

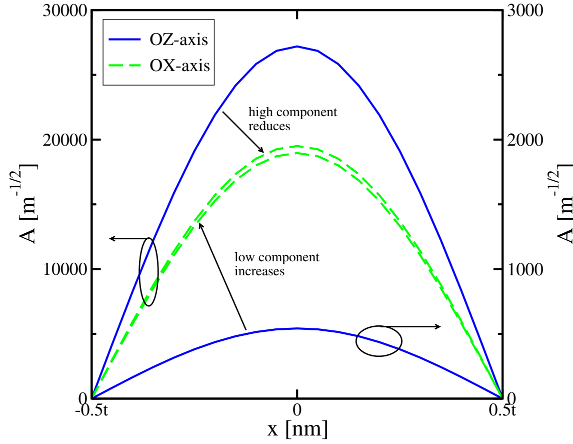

Fig. 1. Absolute value of the large (small) component of the spin wave functions reduces (increases), when the spin injection changes from OZ- to OX-direction. $k_x = 0.4\,\text{nm}$, $k_y = 0.4\,\text{nm}$, and $\varepsilon_{xy} = 0.5$ % kept.

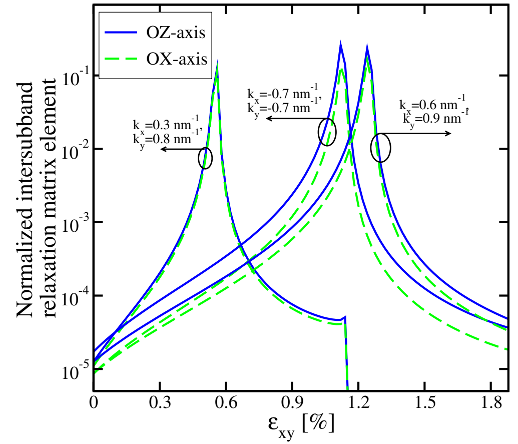

Fig. 2. Normalized intersubband relaxation spin matrix elements (3) as a function of ε_{xy} for spin injection in OX- and OZ-directions, showing a clear reduction for the former case.

strain. p_x and p_y signify the projections of the in-plane momentum. The shear strain can lift the degeneracy between the unprimed subbands [14], which substantially improves the spin lifetime.

Table: Parameter List	
Parameter	Value
Spin-orbit term	$\triangle_{SO} = 1.27\,\text{meVnm}$
Electron rest mass in silicon	$m_e = 9.1093 \cdot 10^{-31}\,\text{Kg}$
Transversal effective mass	$m_t = 0.19\,m_e$
Longitudinal effective mass	$m_l = 0.91\,m_e$
Shear deformation potential	$D = 14\,\text{eV}$

A. Momentum relaxation

The SR induced momentum relaxation rate is calculated in the following way [16], [17]:

$$\frac{1}{\tau_i^M(K_i)} = \frac{2\pi}{\hbar(2\pi)^2} \sum_j \int_0^{2\pi} \pi\triangle^2 L^2 \frac{1}{\epsilon_{ij}^2 \cdot (K_i - K_j)} \frac{\hbar^4}{4m_l^2} \frac{|K_j|}{\frac{\partial E(K_j)}{\partial K_j}} \cdot [(\frac{d\psi_{iK_{i\sigma}}}{dz})^* (\frac{d\psi_{jK_{j\sigma}}}{dz})]^2_{z=\pm\frac{t}{2}} \exp(\frac{-(K_j - K_i)\,L^2}{4})\,\mathrm{d}\phi \tag{2}$$

K_i, K_j are the in-plane wave vectors before and after scattering, ϕ is the angle between K_i and K_j, ϵ is the dielectric permittivity, L is the autocorrelation length, $\triangle$ is the mean square value of the surface roughness fluctuations, ψ_{iK_i} and ψ_{jK_j} are the wave functions, and $\sigma = \pm 1$ is the spin projection to the [001] axis. τ^M represents the SR momentum relaxation time. The SR matrix scattering elements at opposite interfaces are assumed to be independent and proportional to the product of the corresponding subband wave functions' derivative at the interfaces [17].

B. Spin relaxation

The SR induced spin relaxation matrix elements are calculated between the wave functions with opposite spin projections [9]. The spin relaxation matrix elements normalized to the value of the intrasubband scattering at zero strain can be written as:

$$M_{i,j} = [\frac{\frac{d\psi_{i-\sigma}(z)}{dz}\ \frac{d\psi_{j\sigma}(z)}{dz}}{(\frac{d\psi_{i\sigma}(z)}{dz}\ \frac{d\psi_{i\sigma}(z)}{dz})_{\varepsilon_{xy}=0}}]_{z=\pm\frac{t}{2}} \tag{3}$$

where $\psi_{i,j}$ are the subband eigenfunctions and $\sigma = \pm 1$ is the spin projection to the [001] axis. The spin relaxation rate, similar to (2), is expressed as [15], [16]:

$$\frac{1}{\tau_i^S(K_i)} = \frac{4\pi}{\hbar(2\pi)^2} \sum_j \int_0^{2\pi} \pi\triangle^2 L^2 \frac{1}{\epsilon_{ij}^2 \cdot (K_i - K_j)} \frac{\hbar^4}{4m_l^2} \frac{|K_j|}{\frac{\partial E(K_j)}{\partial K_j}} \cdot [(\frac{d\psi_{iK_{i-\sigma}}}{dz})^* (\frac{d\psi_{jK_{j\sigma}}}{dz})]^2_{z=\pm\frac{t}{2}} \exp(\frac{-(K_j - K_i)\,L^2}{4})\,\mathrm{d}\phi \tag{4}$$

τ^S denotes the SR spin relaxation time.

III. Results

A. Increase in spin relaxation time

We look at the subband four-component wave functions for two valleys and two spin projections for different spin injection directions. For perpendicular-plane spin injection the up(down)-spin wave function consists of majority (large) and minority (small) components [14], and their absolute values depend on the shear strain ε_{xy}. When a fixed ε_{xy} and in-plane wave vector (k_x, k_y) is maintained, we find that the absolute value of the majority (minority) component reduces (increases), when the spin injection direction is changed from

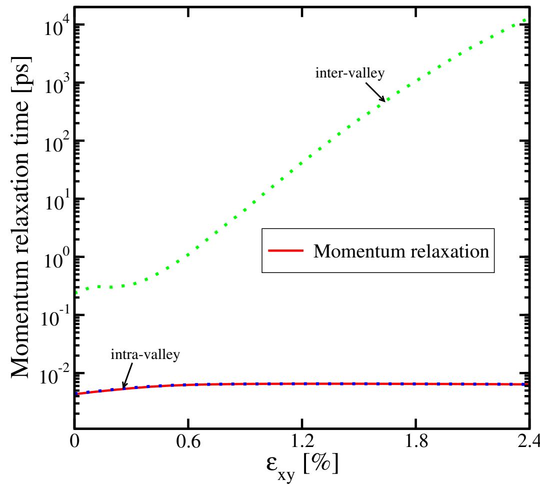

Fig. 3. Variation of momentum relaxation time (2) with ε_{xy} showing no influence of the spin injection direction.

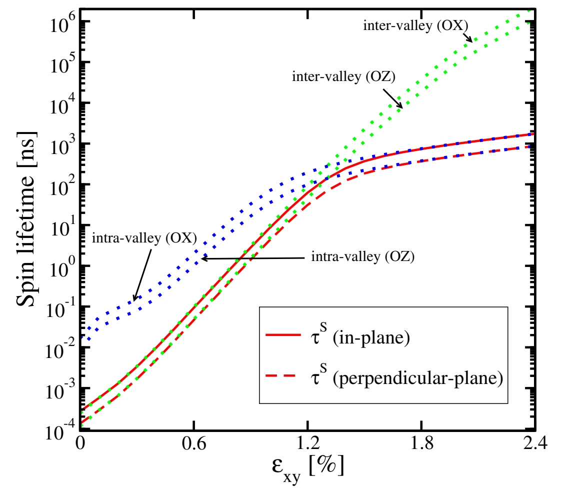

Fig. 4. Variation of spin relaxation time (4) with ε_{xy}, showing inter- and intra-valley components.

perpendicular (OZ-direction) to in-plane (say, OX-direction), Figure 1. However, under these conditions we notice in Figure 2 that the intersubband relaxation matrix elements are reduced, for an in-plane spin injection in OX-direction, compared to the perpendicular-plane spin injection in the OZ-direction. Figure 2 also reveals that for higher shear strain values the hot spots are pushed to higher energies (as energy increases with k_x^2 and k_y^2 increased).

Now we compute the momentum relaxation time with its components (Figure 3), which stays nearly unaltered irrespective of the spin injection direction. The dominance of the intra-subband relaxation process is in agreement with the selection rule that the elastic processes result in strong intra-subband momentum relaxation. We proceed further to evaluate the spin relaxation calculations. As a consequence of Figure 2, it is noticed that the spin relaxation rate is reduced and the corresponding spin lifetime (τ^S) is increased over a large range of ε_{xy}, once spin is injected in-plane as shown in Figure 4. One can notice that for lower (higher) values of ε_{xy}, the inter(intra)-valley scattering component dominates in determining τ^S. The figure also depicts that both of the inter- and intra-valley components increase proportionally for in-plane spin injection.

B. Spin expectation values at hot spots

To explain the observed increase of the spin lifetime for the in-plane spin injection direction we now discuss the expectation values of the spin projection on the axes which are denoted as σ_X, σ_Y, and σ_Z respectively, and hence the total spin expectation

$$\sigma = \sqrt{\sigma_X^2 + \sigma_Y^2 + \sigma_Z^2} \tag{5}$$

at the spin relaxation hot spots (1). The presence of the properly included spin-orbit field (SOF) acting along (p_x, -p_y) direction is considered. In order to check different spin injection expectation values for a certain ε_{xy}, we vary k_y by using k_x as parameter. For spin injection in OZ-direction we find $\sigma_X = \sigma_Y = 0$, and σ_Z also vanishes at the spin hot spots. Figure 5 illustrates the variation of σ which vanishes at the spin hot spots. On the contrary, when spin is injected in the in-plane OX-direction (Figure 6), we notice at the hot spots:

$$\sigma_X = \sin^2(\arctan \frac{p_x}{p_y}) \tag{6a}$$

$$\sigma_Y = -0.5 \, \sin(2 \, \arctan \frac{p_x}{p_y}) \tag{6b}$$

$$\sigma_Z = 0 \tag{6c}$$

According to (5) the total spin expectation is:

$$\sigma = \sin(\arctan \frac{p_x}{p_y}) \tag{7}$$

Figure 7 portrays the hot spot spin precession for spin injected along OX- and OZ-direction in the presence of the spin-orbit field; and we notice that the spin projection in either axes is always zero, if spin is injected in OZ-direction but not for spin injected in OX-direction. Because of the zero spin expectation value at any pair of (p_x, p_y) resulting in maximal spin randomization, the spin relaxation rate (time) will be strongest (weakest) for perpendicular-plane spin injection. Hence, our results indicate that the spin lifetime can be increased, once spin is injected in-plane.

IV. Conclusion

We have shown that an alteration of the spin injection direction will influence the spin relaxation mechanism and henceforth the spin lifetime in an ultra-thin SOI film. We have used an effective **k·p** Hamiltonian to find the wave functions. We have shown that the surface roughness induced intersubband spin relaxation matrix elements are reduced for an in-plane injection, which causes the spin relaxation rate to decrease and hence the spin lifetime to increase, for a

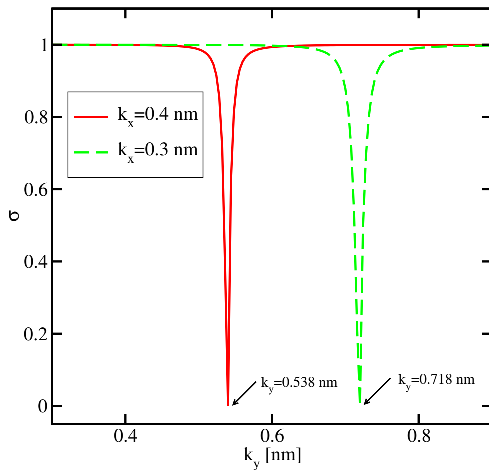

Fig. 5. Total spin expectation σ for perpendicular-plane spin injection along OZ-axis. At hot spots (1), σ goes to zero. $\varepsilon_{xy} = 0.5$ kept.

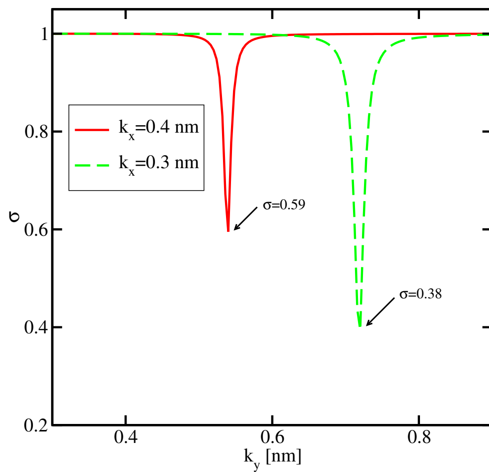

Fig. 6. Total spin expectation σ for in-plane spin injection along OX-axis. At hot spots, σ depends on p_x and p_y (7). $\varepsilon_{xy} = 0.5$ kept.

large range of applied shear strain. We have described that spin experiences a maximal randomization to increase the relaxation rate at the hot spots, if injected perpendicularly; and this results in increasing the lifetime for in-plane injection. We have also shown that, when shear strain is applied, the momentum relaxation time is increased by a factor of two, while the spin lifetime is boosted by orders of magnitude irrespective of the spin injection direction.

Acknowledgment

This work is supported by the European Research Council through the grant #247056 MOSILSPIN.

References

[1] M. Bohr, "The Evolution of Scaling from the Homogeneous Era to the Heterogeneous Era", *Proc. IEDM*, pp. 1.1.1-1.1.6, 2011.

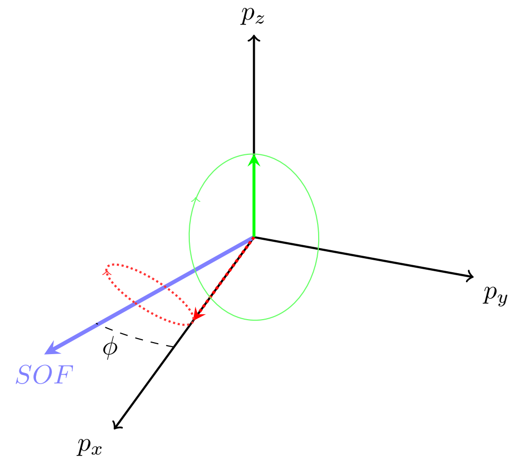

Fig. 7. Precession of the injected spin (along OX- and OZ- direction) around the existing spin-orbit field. $\phi = -\arctan(\frac{p_y}{p_x})$.

[2] D.E. Nikonov and I.A. Young, "Overview of Beyond-CMOS Devices and a Uniform Methodology for Their Benchmarking", *Computer* vol. 36, pp. 15-36, 2013.

[3] M.K. Hudait et al., "Heterogeneous Integration of Enhancement Mode $In_{0.7}Ga_{0.3}As$ Quantum Well Transistor on Silicon Substrate using Thin ($\leq$ 2 μm) Composite Buffer Architecture for High-Speed and Low-voltage (0.5 V) Logic Applications", *Proc. IEDM*, pp. 625-628, 2007.

[4] R. Jansen, "Silicon Spintronics", *Nature Mat.* vol. 11, no. 400, 2012.

[5] B. Huang et al., "Coherent Spin Transport through a 350 Micron Thick Silicon Wafer", *Phys. Rev. Lett.* vol. 99, no. 177209, 2007.

[6] S.P. Dash et al., "Electrical Creation of Spin Polarization in Silicon at Room Temperature", *Nature* vol. 462, pp. 491-494, 2009.

[7] C.H. Li et al., "Electrical Injection and Detection of Spin Accumulation in Silicon at 500 K with Magnetic Metal/Silicon dioxide Contacts.", *Nature Commun.* vol. 2, no. 245, 2011.

[8] J. Li and I. Appelbaum, "Modeling Spin Transport in Electrostatically-gated Lateral-channel Silicon Devices: Role of Interfacial Spin Relaxation", *Phys. Rev. B* vol. 84, no. 165318, 2011.

[9] D. Osintsev et al., "Reduction of Momentum and Spin Relaxation Rate in Strained Thin Silicon Films", *Proc. ESSDERC* pp. 334-337, 2013.

[10] D. Osintsev et al., "Subband Spitting and Surface Roughness Induced Spin Relaxation in (001) Silicon SOI MOSFETs", *Solid-State Electron.* vol. 90, pp. 34-38, 2013.

[11] Y. Song, and H. Dery, "Analysis of Phonon-induced Spin Relaxation Processes in Silicon", *Phys. Rev. B* vol. 86, no. 085201, 2012.

[12] G.L. Bir, and G.E. Pikus, *Symmetry and Strain-induced Effects in Semiconductors*, J. Wiley and Sons, New York/Toronto, 1974.

[13] P. Li, and H. Dery, "Spin-Orbit Symmetries of Conduction Electrons in Silicon", *Phys. Rev. Lett.* vol. 107, no. 107203, 2011.

[14] V. Sverdlov, *Strain-Induced Effects in Advanced MOSFETs*, Springer, 2011.

[15] E. Ungersboeck et al., "The Effect of General Strain on the Band Structure and Electron Mobility of Silicon", *Electron Devices, IEEE Transactions* vol. 54, pp. 2183-2190, 2007.

[16] D. Esseni, "On the Modeling of Surface Roughness Limited Mobility in SOI MOSFETs and its Correlation to the Transistor Effective Field", *Electron Devices, IEEE Transactions* vol. 51, pp. 394-401, 2004.

[17] M.V. Fischetti et al., "Six-band **k**·**p** Calculation of the Hole Mobility in Silicon Inversion Layers: Dependence on Surface Orientation, Strain, and Silicon Thickness", *J. Appl. Phys.* vol. 94, no. 1079, 2003.